Nano Research
2019, 12(4): 815–821

ISSN 1998-0124 CN 11-5974/O4
https://doi.org/10.1007/s12274-019-2293-z

Research Article

Red/orange dual-emissive carbon dots for pH sensing and cell imaging

Miaoran Zhang[1], Rigu Su[1], Jian Zhong[2,3], Ling Fei[4], Wei Cai[1], Qingwen Guan[1], Weijun Li[1], Neng Li[5], Yusheng Chen[6], Lulu Cai[2] (✉), and Quan Xu[1] (✉)

[1] *State Key Laboratory of Heavy Oil Processing, Beijing Key Laboratory of Biogas Upgrading Utilization, China University of Petroleum (Beijing), Beijing 102249, China*
[2] *Personalized Drug Therapy Key Laboratory of Sichuan Province, Department of Pharmacy, Sichuan Provincial People's Hospital, University of Electronic Science and Technology of China, Chengdu 611731, China*
[3] *School of Pharmacy, North Sichuan Medical College, Nanchong 637000, China*
[4] *Chemical Engineering Department, University of Louisiana at Lafayette, Lafayette, LA 70504, USA*
[5] *State Key Laboratory of Silicate Materials for Architectures, Wuhan University of Technology, Wuhan 430070, China*
[6] *Department of Chemistry, University of Akron, Akron, OH 44325, USA*

Received: 2 November 2018 / **Revised:** 3 January 2019 / **Accepted:** 4 January 2018

ABSTRACT

The dual-emissive N, S co-doped carbon dots (N, S-CDs) with a long emission wavelength were synthesized via solvothermal method. The N, S-CDs possess relatively high photoluminescence (PL) quantum yield (QY) (35.7%) towards near-infrared fluorescent peak up to 648 nm. With the advanced characterization techniques including X-ray photoelectron spectroscopy (XPS), Fourier transform infrared spectroscopy (FTIR), etc. It is found that the doped N, S elements play an important role in the formation of high QY CDs. The N, S-CDs exist distinct pH-sensitive feature with reversible fluorescence in a good linear relationship with pH values in the range of 1.0–13.0. What is more, N, S-CDs can be used as an ultrasensitive Ag^+ probe sensor with the resolution up to 0.4 μM. This finding will expand the application of as prepared N, S-CDs in sensing and environmental fields.

KEYWORDS

carbon cell imaging, dual-emissive, photoluminescence, pH-sensitive, Ag^+ probe

1 Introduction

Carbon dots (CDs), a new class of nanomaterials as a replacement of conventional semiconductor quantum dots, have emerged in the past decade and attracted extensive attention [1]. Its excellent properties include low toxicity, simple and low-cost synthesis process, high biocompatibility, and excellent fluorescent properties. Since the discovery of CDs, their fluorescent properties have been widely utilized for detection probes, biomedical imaging, sensing, catalysis, anti-counterfeiting, drug delivery, photovoltaic devices, energy conversion, etc. [2–6]. For example, emerging researches have shown that fluorescence-based nanosensors have become more and more important in the fields of life sciences and environmental sciences due to their fast response and high spatial resolution, which will remain as one of the frontier fields in today's materials science research. In addition to its important role in environmental monitoring and *in vivo*/*vitro* bioanalysis, CD-based nanosensors have also been developed for accurate measurement of pH and Ag^+. Nie et al. reported a ratio metric pH sensor using CDs with two emission wavelengths, which is independently referenced and applied to the measurement of intracellular pH values and cancer diagnosis [7]. Liu et al. reported a green and convenient anhydrous method for the synthesis of fluorescent hydrophilic CDs which exhibit excellent reversible pH-sensitive property between 3.0–13.0 [8]. Gao et al. synthesized a water-soluble carbon nanodots by simple one-step heat treatment of ethylene glycol solution and Ag^+ [9]. The obtained CDs show much enhanced photoluminescence [10]. However, most of the reported CDs stay in blue, green or yellow luminescence with low quantum yield under the excitation of ultraviolet (UV) light [11], and only a few examples of red-emissive CDs have been reported. Blue, green or yellow CDs are unfavorable for biological applications because of the harm of their short wavelength excitation light to biosystems or living cells [12]. On the contrary, red-emitting CDs with long wave length can distinctly broaden the applications ranges, especially in photothermal therapy, fluorescence sensing, optoelectronic conversion, bioimaging, photocatalysis, etc. Therefore, it is highly desirable and a great challenge to develop an effective and straightforward strategy to prepare red-emission CDs with higher quantum yield.

Recently, there are some reported red emission CDs, for example, Sun et al. reported a synthesis of multiple-color-emission CDs by controlled graphitization and surface function, but only obtained a low photoluminescence QY of 12.9% from the red emission CDs [2]. Ding et al. produced efficient red emissive CDs with a PL peak at 625 nm synthesized from urea and p-phenylenediamine through hydrothermal method followed by column chromatography [13]. Fan et al. successfully improved the red fluorescent CDs QY of more than 50% [14]. However, those prepared CDs hardly meet the critical requirements for applications given either having low QY or requiring ethanol as solvent. Thus, it is very important to continue effort on the development of water soluble and long wavelength red CDs which have high quantum yield and can keep their own properties and advantages when used in different solvents. Xu et al. has demonstrated the heteroatom doping is an advanced strategy to

Address correspondence to Lulu Cai, cailulu@med.uestc.edu.cn; Quan Xu, xuquan@cup.edu.cn

enhance the QY of CDs without changing the sizes of CDs and retain their PL properties [15].

Here, we are the first to report the use of N, S co-doping strategy to prepare red-emission N, S-CDs with high quantum yield on pH sensor, Ag^+ detection, and cell imaging. For the synthesis, a solvothermal route was designed with o-phenylenediamine, L-cystine and ethanol as raw ingredients. Among them, o-phenylenediamine is not only the carbon source, but also provides amino functional species for the fluorescent CDs to achieve excellent photo stability. The synthesized CDs have small size around 2.97 nm, which show excitation independent behavior and red fluorescence with the (maximum) emission peak at 595 and 648 nm, and possess relatively high quantum yield (35.7%). When used for pH sensing, the N, S-CDs exhibit excellent pH-responsive and reversible fluorescence in the wide PH value window of 1.0–13.0, which enables the application of N, S-CDs as a potential fluorescent pH sensing probe for environmental samples and living cells. Another exciting finding is that the red fluorescent carbon dots undergo fluorescence quenching under the presence of Ag^+, which allows the CDs to be used as rapid and ultrasensitive detector of Ag^+. Besides pH sensing and Ag^+ detection, it also shows great potential for cell imaging. When incubated in 293T cells, the N, S-CDs not only exhibited high biocompatibility, but also largely enhanced the cell imaging quality. Given the simple synthetic method and excellent performance for various applications, our findings directly contribute to advancing the knowledge of both N, S-CDs synthesis and applications.

2 Experimental section

2.1 Materials

o-Phenylenediamine and L-cystine were obtained from Tianjin Fuchen chemical reagent factory and Energy Chemical Reagent Co., Ltd., respectively. NaOH, HCl, $CuSO_4$, $HgCl_2$, NaCl, $MgCl_2$, $MnCl_2$, $AlCl_3$, $FeCl_3$, $AgNO_3$ and other metal salts used in the sensing application section were purchased from Tianjin Guangfu Technology Development Co., Ltd. All the above reagents are analytical grade and used without further purification in the experiments. Deionized water was produced by BK-10B from Dongguanshi Qianjing environmental equipment Co., Ltd.

2.2 Synthesis of N, S-CDs

In this study, the N, S-CDs were synthesized by solvothermal method. First, L-cystine (0.125 g) and o-phenylenediamine (0.5 g) were dissolved in 20 mL of ethanol, and the solution was transferred into a 50 mL Teflon-lined stainless-steel autoclave. Subsequently, the autoclave was kept in an oven at 220 °C for 12 h and the autoclave was cooled down to room temperature naturally. After that, 2 mL of the original solution of N, S-CDs to 4 mL of NaOH solution (1.25 mol/L), the mixtures were centrifuged at 10,000 rpm for 10 min, the precipitate was added with ethanol to dissolve, then the solution was filtered by a cylindrical filtration membrane filter (0.22 μm) for twice. The solution then went through spin dry in a rotary steaming device to obtain the CDs.

2.3 Characterization of the CDs

The morphology of the as-prepared N, S-CDs was characterized by transmission electron microscopy (TEM; Model JEM-2100). The fluorescence measurements were performed with a fluorescence spectrophotometer (FS5 from Techcomp (China) Ltd.). A fluorescence spectrometer (FLS980) from Techcomp (China) Ltd. was used to measure the photoluminescence quantum yield. Rotary steaming device was from Shanghai Yarong Biochemical Instrument Factory (RE-5298). First, the sample (10 μL of purified N, S-CDs solution diluted to 2 mL, with an absorption lower than 0.05 a.u.) was excited at 540 nm, and the emission spectrum in the range of 550 to 800 nm was measured. Then, 2 mL distilled water (blank sample) was measured under the same conditions. Finally, by comparing the sample and blank sample, the absolute quantum yield of N, S-CDs was calculated. The slit width was fixed at 7.5 and 0.75 nm for excitation and emission, respectively. X-ray photoelectron spectroscopy (XPS) analysis was carried out using an ESCALAB 250 spectrometer with a monochromatic X-ray source Al Kα excitation (1,486.6 eV). Fourier transform infrared spectroscopy (FTIR) spectra were recorded on a Bruker Vertex 70 v.

2.4 Detection of the of Ag^+

The process of detecting Ag^+ using N, S-CDs as a fluorescent probe was carried out as follows. 50 μL N, S-CDs were diluted to 10 mL with deionized water, and then the fluorescence intensity of the solution was measured and defined as the initial fluorescence intensity (F_0). Subsequently, 50 μL N, S-CDs solution was sequentially added to 10 mL of different concentrations of Ag^+ solution and thoroughly mixed to equilibrate (the concentration of N, S-CDs in the mixed solution is 25 μg/mL). The fluorescent intensity (F_1) of the mixture were measured after 5 min. The change of fluorescent intensity is defined as ΔF ($\Delta F = F_0 - F_1$).

2.5 Fluorescent assay of pH

N, S-CDs solutions with different pH value were prepared by adding 20 μL of purified N, S-CDs solution into 2 mL phosphate buffered saline (PBS) with a variety of pH. Then, the fluorescence spectra were recorded 3 min later in the wavelength range of 500–750 nm at an excitation wavelength of 600 nm. All the measurements were repeated three times and then averaged. The fluorescence intensities of N, S-CDs were used to evaluate the pH value in PBS buffers.

2.6 Cell imaging

To observe the influence of carbon dots on cell imaging, 293 T cells were seeded into a 6-well plate with a 12 mm cover slide and cultured at 37 °C for 24 h. Then, different concentrations of N, S-CDs (0, 1,000, and 2,000 μg/mL) were separately added in each well. After the incubation for 8 h at 37 °C, the supernatant was removed, and the cell was washed with PBS for three times and refilled with 4% paraformaldehyde. Images were captured with a confocal microscope (Zeiss LSM880 confocal) and 540 nm was used as excitation wavelength to measure the fluorescence intensity of N, S-CDs. The animal study protocol was approved by the Institutional Animal Care and Use Committee at University of Electronic Science and Technology of China.

2.7 Hemolysis assay

Fresh blood from mice with heparin sodium was taken as anticoagulant and then diluted with PBS (pH = 7.4) solution. The diluent was centrifuged at 2,000 rpm for 5 min, then resuspended in PBS. After centrifugation, the supernatant was removed until the supernatant became colorless and transparent. The red blood cells were made into 2% cell suspension with PBS. Different concentrations of N, S-CDs (0, 1,000, and 2,000 μg/mL) were added to 2% erythrocyte suspension (ESD) and incubated at 37 °C for 4 h, where 1% Triton X-100 was used as positive control and PBS as negative control. Afterward, the centrifugal (EP) tubes were arranged according to the concentration of N, S-CDs and photographed. The solution without red blood cells and with N, S-CDs was used as control to eliminate the interference of the color of the N, S-CDs. The absorption value of supernatant was measured at 490 nm (BioTek CYT3MFV).

2.8 The cell cytotoxicity of N, S-CDs

293T cells were inoculated into 96 well (104 per well) plates and cultured under 5% CO_2 at 37 °C. Different concentration of N,

S-CDs (0–2,000 μg/mL) was added to each well for 24 h, then 20 μL 3-(4,5-dimethylthiazol-2-yl)-2,5-diphenyltetrazolium bromide (MTT) solution (5 mg/mL) was added to each well for 4 h. The supernatant was removed, then 150 mL dimethyl sulfoxide (DMSO) was added into each well. The plate was placed on a bed and shaked for 15 min. Finally, the absorbance was determined by microplate readers (BioTek CYT3MFV) at 570 nm.

3 Results and discussion

The synthesis routes of CDs are mainly divided into two types, top down approach which downsizes bulk materials into small pieces and bottom up which builds up structure from carbon-containing precursors. In this study, the solvothermal treatment, L-cystine and o-phenylenediamine (mass ratio of 1:4) were dissolved in ethanol and kept at 220 °C for 12 h. The reaction yielded a dark red-colored solution, which implied the production of N, S-CDs. The product was filtered using a cylindrical filter membrane filter (0.22 μm) to obtain purified N, S-CDs (Fig. 1(a)). Figures S1 and S2 in the Electronic Supplementary Material (ESM) show the contour plot and three-dimensional (3D) map of corresponding photoluminescence spectrum of N, S-CDs. Figure S3 in the ESM shows the results of UV–visible (UV–vis) spectra, photoluminescence (PL) emission, and PL excitation spectra taken along the horizontal and vertical dash line in the corresponding excitation–emission matrix in Fig. S1 in the ESM. In the process of research, we found that the fluorescence intensity decreases as the pH value of the solution increases, which indicates that the synthesized N, S-CDs possess good pH response property. As shown in Fig. 1(d), the excitation intensity at 560 nm decreases notably as the pH value increases from 1 to 13, and there is a linear relationship when pH is less than 3. In other words, it means the high sensitivity of N, S-CDs towards pH value, as the fluorescent intensity is significantly reduced when the pH changes from 1.0 to 13.0 with NaOH, and it can be restored when reverting the pH from 13.0 to 1.0 with HCl. More strikingly, we can not only observe the linear change of fluorescence intensity at different pH value under the excitation of 600 nm, but also observe the color change of the solution at different pH under UV light (Fig. S8 in the ESM). Notably, the PH value between 1.0 and 2.0, the fluorescent intensity is very strong, however, at the pH of 3, it suddenly reduces and shows almost no fluorescence in the pH range of 8.0 to 13.0,. After 10 times of changing the pH from 1.0 to 13 and then back to 1.0 again, the fluorescent intensity does not change much from the origin value under at the same conditions (Fig. 1(e)), which shows the synthesized N, S-CDs have excellent reversible pH performance and the N, S-CDs can be used in the detection of extreme acid. The steady and robust fluorescence of N, S-CDs in extreme acid solution shows promising material candidates for biomedicine and environmental applications. Figures 1(b) and 1(c) display the PL emission spectra of N, S-CDs dispersed in ethanol solution and acid solution (pH = 1).

The fluorescence spectra of CDs in ethanol show a typical excitation independent PL behavior, with a maximum at 595 and 648 nm, respectively, while in acid it shifts towards read at 625 and 675 nm. This suggests that different environmental conditions have an important influence on the optical properties of CDs. Fluorescence spectra of the N, S-CDs at different precursor ratios of L-cystine and o-phenylenediamine were summarized in Fig. S9 in the ESM. More detailed comparison of the PL properties of N, S-CDs in water, ethanol and acid is available in Fig. S10 in the ESM. It was found that the PL intensity of the N, S-CDs decreases from ethanol, acid to water. It also shows that the emission position of the N, S-CDs is highly sensitive to solvent polarity, which can be attributed to their small size in Fig. S5 in the ESM. We can obviously see that the PL characteristics of N, S-CDs remain almost unchanged, indicating

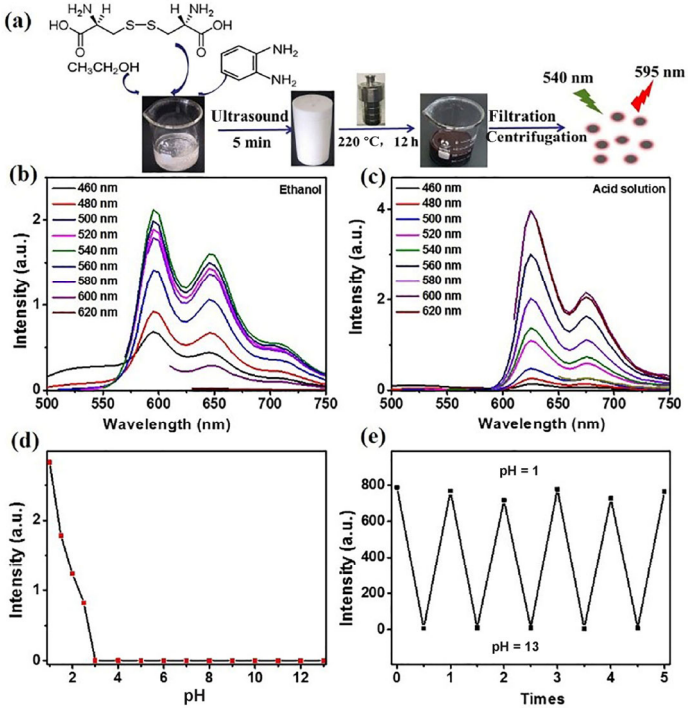

Figure 1 (a) Schematic of the synthesis of N, S-CDs with red luminescence (excited by the light of 540 nm); (b) photoluminescence spectra of the N, S-CDs; (c) photoluminescence spectra of the N, S-CDs in acidic solutions; (d) a linear relationship between the fluorescent intensity and pH (1.0–3.0) (excitation at 600 nm); (e) the reversible pH-response of the fluorescence behavior of N, S-CDs between pH 1.0 and 13.0 (excitation at 600 nm).

that their unique PL characteristics can be used in a variety of applications in these solvent systems. The UV–vis absorption spectra of the as-obtained mixture in Fig. S7 in the ESM display a noticeable peak at 273 and 385 nm, respectively, which is usually assigned to the π–π* transitions of the C=C bonds and the n–π* transition of conjugated C=O and C=N. However, in the lower-energy region from 500 to 650 nm, some new absorption bands appear at 530 and 571 nm in ethanol solution and three more absorption peaks appear at 510, 590 and 630 nm in acidic solutions. The band at 571 nm is mainly assigned to the n–π* transition of the conjugated C=S bond. These new peaks are attributed to n–π* transitions of the aromatic sp^2 system containing C=O and C=N bonds, the C=C bonds, and the n–π* transition of conjugated C=O and C=N [13]. Additionally, in the lower-energy region from 500 to 650 nm, some new absorption bands appear at 530 and 571 nm in ethanol solution and three more absorption peaks appear at 510, 590 and 630 nm in acidic solutions. The band at 571 nm is assigned to the n–π* transition of the conjugated C=S bond. These new peaks are attributed to n–π* transitions of the aromatic sp^2 system containing C=O and C=N bonds. The PL excitation spectra of CDs show that the emission was mainly generated by the absorption bands from the n–π* transition of the aromatic sp^2 system containing C=O and C=N bonds [2, 4]. The emission peaks of N, S-CDs are centered at 595 and 628 nm, respectively. Especially, the self-absorption of N, S-CDs in both solutions is quite small as indicated by the small overlap between excitonic absorption and emission spectrum, which is advantageous for efficient fluorescence emission. The hypothesis can be further confirmed by the PL decay measurement (Fig. S4 in the ESM). The results show that the PL decay curves of N, S-CDs in both environments are very similar. The resultant lifetimes are 6.25 and 3.08 ns for N, S-CDs in ethanol and acid solution, respectively. The decrease of lifetime of the N, S-CDs treated at acidic conditions can be correlated with the nature of the doped elements at that corresponding environment.

The particle size and structure analysis of the as-prepared CDs were investigated using both transmission electron microscopy (TEM) and atomic force microscopy (AFM). A dilute aqueous solution of N, S-CDs was drop-casted on mica substrates for AFM investigation and on a carbon coated copper grid for TEM measurement (Fig. 2(a)). The N, S-CDs in ethanol solution show a spherical morphology and a narrow size distribution from 2 to 5 nm with the average around 2.97 nm (Fig. 2(b)). About 80% of the N, S-CDs are between 2.5 and 3.5 nm, indicating the high level of size selectivity of the synthetic process. Figure S5 in the ESM shows that the N, S-CDs diameter is less than 1 nm in the acidic solution. The AFM images (Fig. 2(d) and Fig. S13 in the ESM) further demonstrated that the N, S-CDs are quasi-spherical in different solvents, which provide a relatively precise thickness. The thickness distributions indicate that the average thicknesses of N, S-CDs in ethanol and acid solution are 2.69 and 1.83 nm, respectively.

To obtain details about the surface chemistry and collect insights on robust mechanisms, N, S-CDs were analyzed using FTIR (Fig. 2(c)) and XPS (Fig. 3). As seen in Fig. 2(c), the bonds of N, S-CD in ethanol and acidic solution in the FTIR spectra are very similar, except the vibrational intensity of the peak is different. The FTIR spectra of N, S-CDs in both ethanol and acid solutions have obvious characteristic peaks between 3,000–3,500 cm^{-1}, which can be attributed to H–O and N–H bonds, indicating that there are plenty of hydroxyl groups on the surface of CDs.

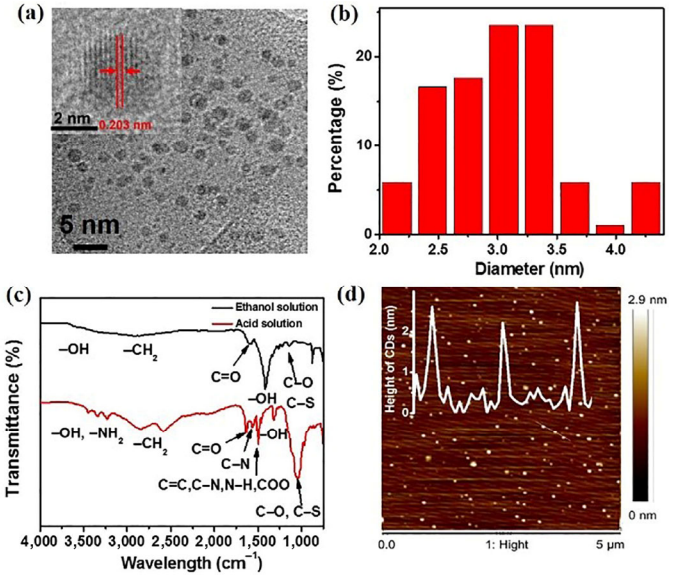

Figure 2 (a) TEM image of N, S-CDs; (b) the diameter distribution of N, S-CDs calculated from TEM image; (c) FT-IR spectra of N, S-CDs in different solvents; (d) AFM image of the N, S-CDs.

These functional groups directly contribute to the highly hydrophilic nature of N, S-CDs [16–18]. Compared to ethanol solution, the spectrum of the N, S-CDs in the acid solution shows that the stretching vibrations at 1,513 cm^{-1} and the intensity of C–O, C–S vibrations at 1,060 cm^{-1} are enhanced, while the intensity of H–O and N–H vibrations are reduced. This result implies that N, S-CDs in acid have relatively more C=C and C–N bonds and fewer O–H bonds. The strong bands at 1,513 cm^{-1} is ascribed to the C=C, C–N, N–H and COO^- stretching vibrations [19, 20]. The distinct absorption bands located at 1,589 and 1,563 cm^{-1} can be attributed to the vibration of C=O and C–N, respectively [21, 22]. The difference of FTIR spectra between ethanol and acid was resulted from the solvent effect. N, S-CDs exhibited higher solubility in ethanol than acid aqueous solution. Due to the stronger interaction between ethanol molecule and CDs by polar–polar or van der Waal force, ethanol has higher affinity towards CDs surface, which broadens the peaks in the FTIR. In acid solution, due to the lower solubility, the solvent effect was not found to have less impact on the FTIR spectrum, which leads to the observation of the subtle structure of C–H stretch at 2,750 cm^{-1}. It can be concluded that the size of N, S-CDs decreased, and the number of N–H bonds reduced in acidic solutions. Figure S7 in the ESM shows the UV–vis absorption spectra of N, S-CDs in ethanol and acid solution, respectively, the absorption of N, S-CDs in acid is larger than that in ethanol in the band of 400–650 nm, which should also be attributed to the protonation and deprotonation of surface groups. The acid is positively charged, so at lower pH, the protonation of the CDs is more electrophilic, hindering the CDs from growing further, and the strong vibrational coupling of the OH functional groups, caused by H-bonding effects, can lead to the energy level broadening and increase the conformational rigidity of CDs, thereby affecting the size and fluorescence properties of N, S-CDs [3, 23].

The presence of C–N, N–H, C–S, S–H, C=C, C=O, and C–N was also confirmed by XPS spectra (Fig. 3). Figure 3 illustrates the high-resolution C 1s, N 1s, O 1s and S 2p XPS spectra of CDs dissolved

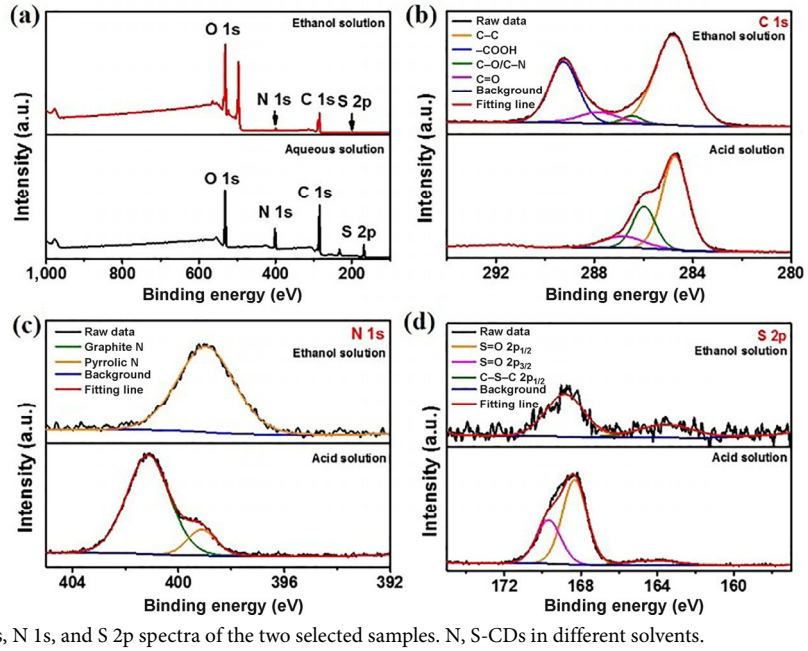

Figure 3 High-resolution XPS C 1s, N 1s, and S 2p spectra of the two selected samples. N, S-CDs in different solvents.

in different solutions. The full spectra presented in Fig. S6 in the ESM show four typical peaks: C 1s (285 eV), O 1s (531 eV), S 2p (168 eV), and N 1s (400 eV). The content of C, N, S, and O elements in N, S-CDs was surveyed from the XPS spectrum (Table S1 in the ESM). It is clearly shown the presence of C (43.03 %), N (0.51%), S (3.69%) and O (52.78%) in the ethanol and the presence of C (51.09%), N (14.87%), S (7.16%) and O (26.88%) in the acidic solution of N, S-CD, respectively. In the Fig. 3(b), the C 1s band of the CDs that used ethanol as a solvent, can be deconvoluted into four peaks, corresponding to sp^2 carbons (C–C/C=C, 284.77 eV), carbonyl carbons (C=O, 287.82 eV), sp^3 carbons (C–O/C–N, 286.43 eV), and carboxyl carbons (COOH, 289.26 eV). The XPS intensity at 286.43 eV gradually increases and at 289.26 eV disappears from ethanol to acid indicating a corresponding increase C–O/C–N bonds reduce in the content of carboxyl groups in the CDs, which consistent with the FTIR results. The N 1s spectrum has one distinct peak located at 398.99 eV, representing the pyridinic N. The S 2p band can be deconvoluted into peak at 168.7 eV and assigned to –C–SO_x–C– sulfone bridges (Fig. 3(d)) [24]. The O 1s band contains two peaks at 531.16 and 531.59 eV for C=O and C–O, respectively (Fig. S6 in the ESM). The XPS spectrum of N, S-CD under acidic conditions is like that of ethanol diluted N, S-CD. Figure 3(b) show that when acid is used as solvent, the C 1s band can be deconvoluted into three peaks, corresponding to sp^2 carbons (C–C/C=C, 284.8 eV), carbonyl carbons (C=O, 286.63 eV), and sp^3 carbons (C–O/C–N, 285.59 eV). The N 1s spectrum has one distinct peak located at 401.13 eV, representing pyridinic N. The O 1s band and S 2p band in both environments are the same [25]. The atomic ratio between oxygen and carbon decreases from 1.21 to 0.52 as the O content decreases from 52.78% to 26.88% for ethanol to acid (Tables S1 in the ESM), reflecting the same tendency in the degree of oxidation reduced of the CDs, consistent with the FTIR results. Meanwhile, the N peak shift from pyrrolic N to graphic N in acid condition, indicating the H^+ can form electronic interaction with CDs. This interaction especially occurred in the N atom, rather than S atom, due to nitrogen lone pairs. There is possibility that the interaction exists between neighboring nitrogen atom and incorporates the conjugated system of graphic N–C on the CDs' surface, which is one of reasons for the photoluminescence red shift (Figs. 1(b) and 1(c)).

Silver is one of the trace elements in human tissues and is usually present Ag^+ in an aqueous solution. The solution is colorless and transparent without any solid particles. Trace amount of silver is harmless to the human body, and silver ions have a strong antibactericidal effect. However, Ag^+ metabolites may cause a series of side effects such as silver poisoning and silver accumulation [26]. For our environment and health, we need to find an easy way to detect silver ions. Compared with colorimetry, electrochemical methods and so on [11, 27], using CDs to detect Ag^+ has the advantages of quick response and simplicity. To evaluate the response speed of the Ag^+ sensor, time-dependent fluorescence quenching of N, S-CD in the presence of Ag^+ (50 μM) at different times was compared, and fluorescence intensity decreased by 56.5% after quenching. It shows that the fluorescence of as-prepared N-CDs has incredibly fast response on Ag^+ (Fig. 4(a)). The influence of Ag^+ with different concentrations on the fluorescence intensity of N, S-CDs was also investigated. As shown in Fig. 4(c), the concentration of Ag^+ in the range of 0 to 100 μM had a good linear relationship with the fluorescence quenching degree of N, S-CDs ($\Delta F = 0.01149C + 0.0843$, $R^2 = 0.9913$).

To evaluate the selectivity of the proposed Ag^+ sensor, the detection of Ag^+ was carried out in the presence of various mono, di, and trivalent ions. In detail, 50 μM of various metal ions, including Na^+, Mn^{2+}, K^+, Cu^+, Fe^{3+}, Ag^+, Cu^{2+}, Al^{3+} and Zn^{2+} were added to the N, S-CDs solution, and the changes of fluorescence intensity (ΔF) at 540 nm for N, S-CDs in the presence of various metal ions were

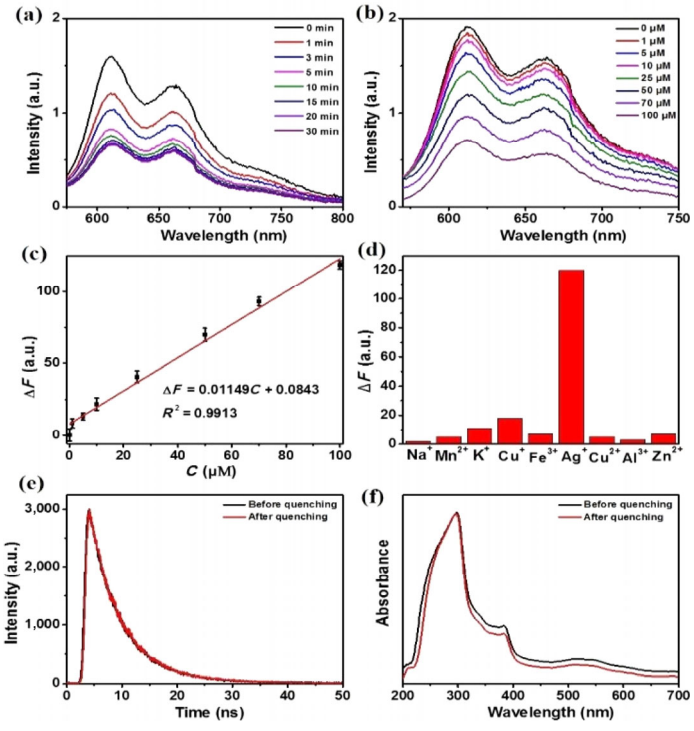

Figure 4 (a) Time-dependent fluorescence changes of N, S-CDs in the presence of Ag^+ (50 μM); (b) emission spectra of the CDs solution with different concentrations of Ag^+ (0–100 μM); (c) the change of fluorescence intensity of N, S-CDs solution vs. the concentration of Ag^+; error bars in (c) represent the standard deviations of three independent measurements; (d) the change of fluorescence intensity at 595 nm for N, S-CDs in the presence of the various metal ions; (e) decay before and after quenching of N, S-CDs; (f) absorption before and after quenching of N, S-CDs.

recorded. As demonstrated in Fig. 4(d). The presence of Ag^+ ions in N, S-CDs leads to a significant decrease in fluorescence intensity. But if there are other metal ions in the N, S-CDs, the fluorescence doesn't change significantly. Therefore, it can be concluded that silver ions have a certain selective quenching effect on N, S-CDs. The synthesized N, S-CDs demonstrate obvious fluorescence quenching within a short time, namely, rapid response. This apparent fluorescence intensity change can be attributed to the fact that Ag^+ can facilitate the electron/hole recombination annihilation through an alternative and efficient electron-transfer process, similar to reports by previous research [28]. This electron/hole recombination can lead to the change of morphology and electronic state on the surface of the CDs. Different from the photoluminescence shift induced by H^+/CDs interaction, no shift and peak shape change are observed, which may be due to the weak interaction between Ag^+ and the CDs surface, in accordance with the results of fluorescence life time. The lifetime and absorption of N, S-CDs before and after quenching are almost the same, the results show that the addition of Ag^+ has no effect on lifetime absorption (Figs. 4(e) and 4(f)).

To explain the high yield of the red/orange dual-emissive N, S-CDs, the electronic structure as a function of the dopant in carbon quantum dots was analyzed (Fig. 5(a)). One can see that the S, or N, S-dopants lead to more electronic states, and the creation of in-gap trap states that could act as nonradiative and the creation of recombination centres. This is in line with the trend that is found in the photoluminescence quantum yield (PLQY) as a function of heteroatom doped CDs.

Moreover, to confirm the C–N bonding, the difference effective charge is calculated for the nearest carbon and nitrogen atoms in N, S-CDs, which is shown in the Table S2 in the ESM. For N, S-CDs, one can see that C gets 0.765 electron (e) charges from atoms around. It is notable that, carbon gets a much more charges (0.765 e) compared

to its in S-monodoped CDs (0.561 e), indicating that there are some electron transferred from the nearest nitrogen atom to carbon atom. This agrees well with the experimental observation.

To investigate the cytotoxicity of the N, S-CDs probe toward living cells, 293T cells were selected as a model system to incubate with N, S-CDs, and then the fluorescence of 293T cells at different concentrations were determined (Fig. 6). The red fluorescence is captured under 540 nm excitation wavelengths. The first column is bright field image, and the second and third columns show the images with excitation wavelengths at 500–560 nm and the merged

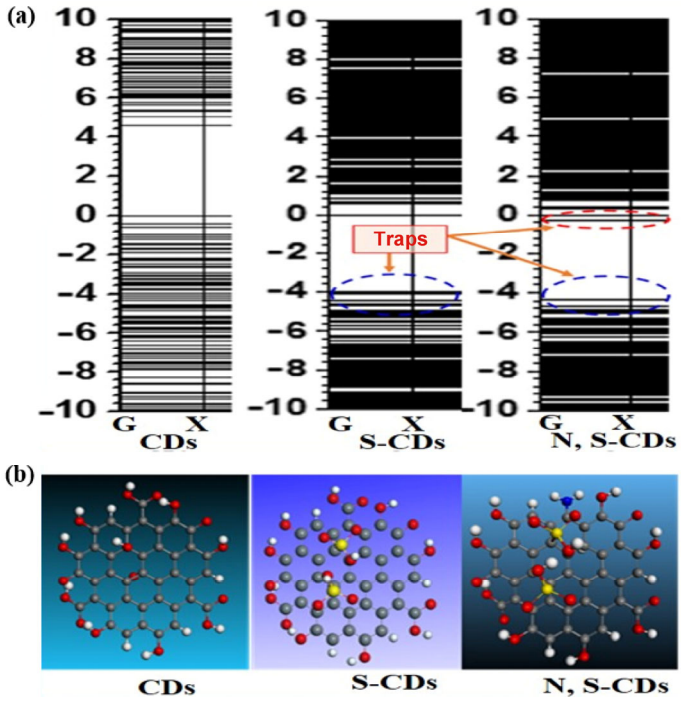

Figure 5 (a) Electronic structure of a CDs, S-monodoped CDs, and N, S-codoped CDs. (b) Relaxed structure, computed at the density functional theory (DFT)/Perdew–Burke–Ernzerhof (PBE) level of theory, for bare CDs, S-monodoped CDs, and N, S-codoped CDs.

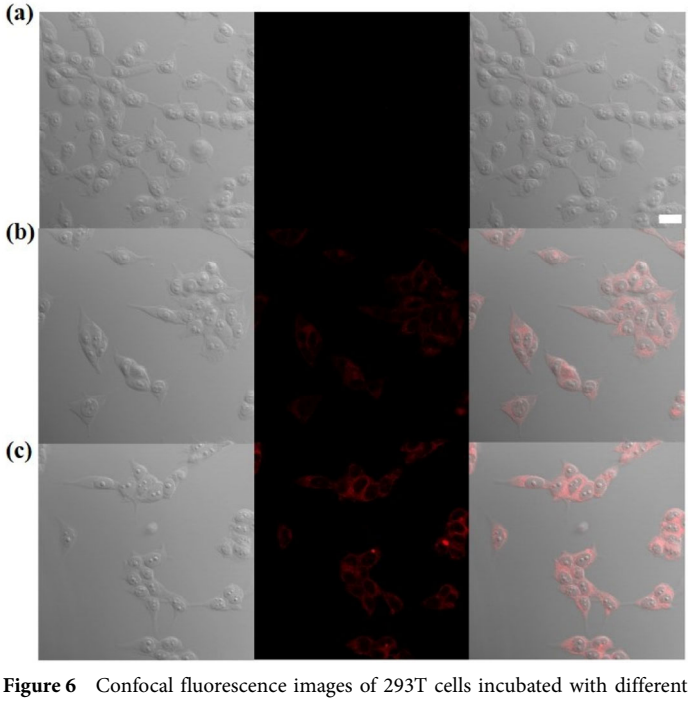

Figure 6 Confocal fluorescence images of 293T cells incubated with different concentrations N, S-CDs at 37 °C for 4 h. (a) Control group; (b) 1,000 μg/mL N, S-CDs; (c) 2,000 μg/mL N, S-CDs; the scale bar is 20 μm.

images of the first and second columns, respectively. From Fig. S11 in the ESM, it could be seen that the cell viability was estimated to be more than 80% upon the addition of N, S-CDs probe with a wide concentration range of 0–1,000 μg/mL. Hereafter, cell imaging experiments were conducted to further demonstrate the availability of the as-prepared N, S-CDs probe for imaging living 293T cells [29, 30]. With the increase of N, S-CDs concentration in the culture medium, gradual increases in the brightness or the intensity of fluorescence images are observed. The comparison chart in Fig. S12 in the ESM shows that the N, S-CDs have only minimal hemolysis behavior. These observations illustrated a close correlation of the fluorescence images intensity with N, S-CDs concentration in the culture medium, which indicate that CDs probes have broad application in biological imaging and Ag^+ detection.

4 Conclusion

In conclusion, N, S-CDs were synthesized through a facile hydrothermal method. Our CDs show rare red/orange dual-emission and have the advantage of easy preparation, low toxicity, and high yield. The as-prepared N, S-CDs with dual emission peaks (595 and 648 nm) under a single excitation without any further modification can be used as fluorescent probe for strong acid sensing and Ag^+ detection. N, S-CDs have excellent reversible pH performance and the N, S-CDs can be used in the detection of extreme acid. In addition, the as-prepared N, S-CDs with a quasi-spherical shape, an average size of 2.97 nm, narrow size distribution and high solution dispersibility demonstrated strong excitation independent emission at 595 nm with a 35.7% quantum yield. The CDs shows excellent detection capability towards Ag^+ over a wide concentration range of 0–100 μM. Hence, the work presents a readily adaptable fluorescence-based protocol which could be applied in environmental, energy, and biomedical fields.

Acknowledgements

We thank Beijing Nova Program Interdisciplinary Studies Cooperative Project (No. Z181100006218138), Science Foundation of China University of Petroleum-Beijing (No. 2462018BJC004), National Key Specialty Construction Project of Clinical Pharmacy (No. 30305030698) and Research Funding of Sichuan Provincial People's Hospital (No. 2017LY08) for the support.

Electronic Supplementary Material: Supplementary material (Figs. S1–S13 and Table S1) is available in the online version of this article at https://doi.org/10.1007/s12274-019-2293-z.

References

[1] Zhu, S. J.; Song, Y. B.; Zhao, X. H.; Shao, J. R.; Zhang, J. H.; Yang, B. The photoluminescence mechanism in carbon dots (graphene quantum dots, carbon nanodots, and polymer dots): Current state and future perspective. *Nano Res*. **2015**, *8*, 355–381.

[2] Miao, X.; Qu, D.; Yang, D. X.; Nie, B.; Zhao, Y. K.; Fan, H. Y.; Sun, Z. C. Synthesis of carbon dots with multiple color emission by controlled graphitization and surface functionalization. *Adv. Mater*. **2018**, *30*, 1704740.

[3] Zhang, Y. B.; Chan, K. F.; Wang, B.; Chiu, P. W. Y.; Zhang, L. Spore-derived color-tunable multi-doped carbon nanodots as sensitive nanosensors and intracellular imaging agents. *Sensors Actuat. B-Chem*. **2018**, *271*, 128–136.

[4] Chen, Y. H.; Zheng, M. T.; Xiao, Y.; Dong, H. W.; Zhang, H. R.; Zhuang, J. L.; Hu, H.; Lei, B. F.; Liu, Y. L. A self-quenching-resistant carbon-dot powder with tunable solid-state fluorescence and construction of dual-fluorescence morphologies for white light-emission. *Adv. Mater*. **2016**, *28*, 312–318.

[5] Zhu, S. J.; Meng, Q. N.; Wang, L.; Zhang, J. H.; Song, Y. B.; Jin, H.; Zhang, K.; Sun, H. C.; Wang, H. Y.; Yang, B. Highly photoluminescent carbon dots for multicolor patterning, sensors, and bioimaging. *Angew. Chem*. **2013**, *52*, 3953–3957.

[6] Li, W.; Zhang, Z. H.; Kong, B.; Feng, S. S.; Wang, J. X.; Wang, L. Z.; Yang, J. P.; Zhang, F.; Wu, P.Y.; Zhang, D. Y. Simple and green synthesis of nitrogen-doped photoluminescent carbonaceous nanospheres for bioimaging. *Angew*. *Chem*. **2013**, *52*, 8151–8155.

[7] Nie, H.; Li, M. J.; Li, Q. S.; Liang, S. J.; Tan, Y. Y.; Sheng L.; Shi, W.; Zhang, S. X. A. Carbon dots with continuously tunable full-color emission and their application in Ratiometric pH sensing. *Chem*. *Mater*. **2014**, *26*, 3104–3112.

[8] Liu, X. X.; Yang, C. L.; Zheng, B. Z.; Dai, J. Y.; Yan, L.; Zhuang, Z. G.; Du, J.; Guo, Y.; Xiao, D. Green anhydrous synthesis of hydrophilic carbon dots on large-scale and their application for broad fluorescent pH sensing. *Sensors Actuat*. *B-Chem*. **2018**, *255*, 572–579.

[9] Gao, X. H.; Lu, Y. Z.; Zhang, R. Z.; He, S. J.; Ju, J.; Liu, M. M.; Li, L.; Chen, W. One-pot synthesis of carbon nanodots for fluorescence turn-on detection of Ag^+ based on the Ag^+-induced enhancement of fluorescence. *J*. *Mater*. *Chem*. *C* **2015**, *3*, 2302–2309.

[10] Miao, P.; Han, K.; Tang, Y. G.; Wang, B. D.; Lin, T.; Cheng, W. B. Recent advances in carbon nanodots: Synthesis, properties and biomedical applications. *Nanoscale* **2015**, *7*, 1586–1595.

[11] Dong, Y. Q.; Chen, Y. M.; You, X.; Lin, W.; Lu, C. H.; Yang, H. H.; Chi, Y. W. High photoluminescent carbon based dots with tunable emission color from orange to green. *Nanoscale* **2017**, *9*, 1028–1032.

[12] Ding, H.; Ji, Y.; Wei, J. S.; Gao, Q. Y.; Zhou, Z. Y.; Xiong, H. M. Facile synthesis of red-emitting carbon dots from pulp-free lemon juice for bioimaging. *J*. *Mater*. *Chem*. *B* 2017, *5*, 5272–5277.

[13] Zhao, A. D.; Chen, Z. W.; Zhao, C. Q.; Gao, N.; Ren, J. S.; Qu, X. G. Recent advances in bioapplications of C-dots. *Carbon* **2015**, *85*, 309–327.

[14] Wang, Z. F.; Yuan, F. L.; Li, X. H.; Li, Y. C.; Zhong, H. Z.; Fan, L. Z.; Yang, S. H. 53% efficient red emissive carbon quantum dots for high color rendering and stable warm white-light-emitting diodes. *Adv*. *Mater*. **2017**, *29*, 1702910.

[15] Xu, Q.; Li, B. F.; Ye, Y. C.; Cai, W.; Li, W. J.; Yang C. Y.; Chen, Y. S.; Xu, M.; Li, N.; Zheng, X. S. et al. Synthesis, mechanical investigation, and application of nitrogen and phosphorus co-doped carbon dots with a high photoluminescent quantum yield. *Nano Res*. **2018**, *11*, 3691–3701.

[16] Zhang, Y.; He, J. H. Facile synthesis of S, N co-doped carbon dots and investigation of their photoluminescence properties. *Phys*. *Chem*. *Chem*. *Phys*. **2015**, *17*, 20154–20159.

[17] Chen, Y. H.; Zheng, M. T.; Xiao, Y.; Dong, H. W.; Zhang, H. R.; Zhuang, J. L.; Hu, H.; Lei, B. F.; Liu, Y. I. A self-quenching-resistant carbon-dot powder with tunable solid-state fluorescence and construction of dual-fluorescence morphologies for white light-emission. *Adv*. *Mater*. **2016**, *28*, 312–318.

[18] Jiang, J.; He, Y.; Li, S. Y.; Cui, H. Amino acids as the source for producing carbon nanodots: Microwave assisted one-step synthesis, intrinsic photoluminescence property and intense chemiluminescence enhancement. *Chem*. *Commun*. **2012**, *48*, 9634–9636.

[19] Xu, Q.; Liu, Y.; Gao, C.; Wei, J. F.; Zhou, H. J.; Chen, Y. S.; Dong, C. B.; Sreeprasad, T. S.; Li, N.; Xia, Z. H. Synthesis, mechanistic investigation, and application of photoluminescent sulfur and nitrogen co-doped carbon dots. *J*. *Mater*. *Chem*. *C* **2015**, *3*, 9885–9893.

[20] Wu, M. B.; Wang, Y.; Wu, W. T.; Hu, C.; Wang, X. N.; Zheng, J. T.; Li, Z. T.; Jiang, B.; Qiu, J. S. Preparation of functionalized water-soluble photoluminescent carbon quantum dots from petroleum coke. *Carbon* **2014**, *78*, 480–489.

[21] Sun, D.; Ban, R.; Zhang, P. H.; Wu, G. H.; Zhang, J. R.; Zhu, J. J. Hair fiber as a precursor for synthesizing of sulfur- and nitrogen-co-doped carbon dots with tunable luminescence properties. *Carbon* **2013**, *64*, 424–434.

[22] Zhang, J.; Yang, L.; Yuan, Y.; Jiang, J.; Yu, S. H. One-pot gram-scale synthesis of nitrogen and sulfur embedded organic dots with distinctive fluorescence behaviors in free and aggregated states. *Chem*. *Mater*. **2016**, *28*, 4367–4374.

[23] Yuan, F. L.; Ding, L.; Li, Y. C.; Li, X. H.; Fan, L. Z.; Zhou, S. X.; Fang, D. C.; Yang. S. H. Multicolor fluorescent graphene quantum dots colorimetrically responsive to all-pH and a wide temperature range. *Nanoscale* **2015**, *7*, 11727–11733.

[24] Gu, W. T.; Sevilla, M.; Magasinski, A.; Fuertes, A. B.; Yushin, G. Sulfur-containing activated carbons with greatly reduced content of bottle neck pores for double-layer capacitors: A case study for pseudocapacitance detection. *Energy Environ*. *Sci*. **2013**, *6*, 2465–2476.

[25] Ding, H.; Wei, J. S.; Xiong, H. M. Nitrogen and sulfur co-doped carbon dots with strong blue luminescence. *Nanoscale* **2014**, *6*, 13817–13823.

[26] Huang, S. S.; He, S.; Lu, Y.; Wei, F. F.; Zeng, X. S.; Zhao, L. C. Highly sensitive and selective fluorescent chemosensor for Ag^+ based on a coumarin-Se_2N chelating conjugate. *Chem*. *Commun*. **2011**, *47*, 2408–2410.

[27] Dang, D. K.; Sundaram, C.; Ngo, Y. L. T.; Chung, J. S.; Kim, E. J.; Hur, S. H. One pot solid-state synthesis of highly fluorescent N and S co-doped carbon dots and its use as fluorescent probe for Ag^+ detection in aqueous solution. *Sensors Actuat*. *B-Chem*. **2018**, *255*, 3284–3291.

[28] Ong, W. J.; Tan, L. L.; Chai, S. P.; Yong, S. T. Heterojunction engineering of graphitic carbon nitride ($g\text{-}C_3N_4$) via Pt loading with improved daylight-induced photocatalytic reduction of carbon dioxide to methane. *Dalton Trans*. **2015**, *44*, 1249–1257.

[29] Liu, J.; Dong, Y.; Ma, Y.; Han, Y.; Ma, S.; Chen, H. One-step synthesis of red/green dual-emissive carbon dots for ratiometric sensitive $ONOO^-$ probing and cell imaging. *Nanoscale* **2018**, *10*, 13589–13598.

[30] Zhang, X. Y.; Wang, S. Q.; Zhu, C. Y.; Liu, M. Y.; Ji, Y.; Feng, L.; Tao, L.; Wei, Y. Carbon-dots derived from nanodiamond: photoluminescence tunable nanoparticles for cell imaging. *J*. *Colloid Interf*. *Sci*. **2013**, *397*, 39–44.